PERGAMON

PII: S1359-6454(99)00011-7

Acta mater. Vol. 47, No. 4, pp. 1105–1115, 1999

Printed in Great Britain
1359-6454/99 $19.00 + 0.00

CRYSTALLOGRAPHY AND INTERFACE BOUNDARY STRUCTURE OF PEARLITE WITH M_7C_3 CARBIDE LAMELLAE

D.V. SHTANSKY†‡, K. NAKAI and Y. OHMORI

Department of Materials Science and Engineering, Ehime University, 3 Bunkyo-cho, Matsuyama 790-8577, Japan

(Received 9 November 1998; received in revised form 22 December 1998; accepted 3 January 1999)

Abstract—The crystallography of pearlite with M_7C_3 carbide lamellae and the atomic structure at the ferrite/carbide interface have been examined by means of transmission electron microscopy in an Fe–8.2Cr–0.96C alloy. Two orientation relationships with the corresponding habit planes were determined: OR-I: $(\bar{2}\bar{5}1)_b//(1\bar{1}\bar{2}0)_{hex}$—habit plane, $(\bar{1}13)_b//(\bar{1}100)_{hex}$, $(\bar{3}\bar{1}\bar{1})_b \approx //(0001)_{hex}$; OR-II: $(\bar{2}\bar{5}1)_b//(1\bar{1}00)_{hex}$—habit plane, $(\bar{1}13)_b//(1\bar{1}\bar{2}0)_{hex}$, $(\bar{3}\bar{1}\bar{1})_b \approx //(0001)_{hex}$. Variants of these orientation relationships have been frequently observed. Microscopic steps at the ferrite/carbide interfaces accommodate the curvature of the habit planes. Each of these orientation relationships provides a small misorientation between the $\{110\}_b$ close packed planes of ferrite and the coincident planes of M_7C_3 carbide, and the atomic planes are perfectly matched through the interface. The orientation relationship between the parent austenite and M_7C_3 carbide was also deduced assuming the ferrite/austenite orientation relationship so far obtained.

1. INTRODUCTION

By definition, pearlite is a lamellar eutectoid structure consisting of ferrite and carbide, which can form from the parent austenite by solid-state reaction under either isothermal or continuous cooling heat treatment. The theory of pearlite reaction has been studied quite intensively because of the importance of pearlite in view of fundamental principles of phase transformations and also in the case of hardenability. Thus, an extensive literature is available concerned with the different aspects of pearlite reactions such as mechanism of pearlite growth [1–4], kinetics [5, 6], effect of alloying elements [7, 8], crystallography [9–11] and interlamellar spacing [12]. The classical theory of pearlite growth based on the results by Hull and Mehl [13], Zener [14] and Mehl and Hagel [15] has been generalized by Hillert [16]. Over the last decade attempts have been made to revise some basic principles of the classical views of pearlite reaction on the basis of new experimental results. Hackney and Shiflet [10] proposed the ledge mechanism of pearlite growth in ferrous alloys that was later confirmed by Whiting and Tsakiropoulos [3] for the Cu–Al lamellar eutectoid. The last results revealed the even greater role of crystallography than those previously accepted although the subject has been recently debated and different points of view were expressed [17, 18]. It should also be noted that Khalid and Edmonds [19] have shown that coarsely spaced linear defects similar to those previously reported by Hackney and Shiflet [1, 10] were not intrinsic growth ledges on these interfaces, but extrinsic defects resulting from intersection of the growing interface with planar stacking faults present in the parent austenite.

Because of the effect of crystallography during the development of pearlite, a unique atomic habit plane is maintained that gives a good correlation between three reported orientation relationships (OR) and their related atomic habit planes:

Bagaryatskii OR [20]
$(001)_{orth}//(11\bar{2})_b$ habit plane [9]
Isaichev OR [21]
$(101)_{orth}//(11\bar{2})_b$ habit plane [22]
Pitsch–Petch OR [23, 24]
$(001)_{orth}//(\bar{2}\bar{1}5)_b$ habit plane [24].

In contrast, four new orientation relationships between pearlitic ferrite and cementite have recently been reported by Zhang and Kelly [11]. They proposed that two widely accepted orientation re-

†Dmitry V. Shtansky, Japan Society Post-Doctoral Fellow, on leave from I.P. Bardin Central Research Institute for Iron and Steel Industry, 2nd Baumanskaja Street, 9/23, Moscow, 107005, Russia.

‡To whom all correspondence should be addressed.

lations, namely the Pitsch–Petch OR and the Bagaryatskii OR probably do not exist.

Whereas the crystallography between pearlitic ferrite and cementite has been studied rather intensively, very little attention has been given to the crystallography between ferrite and alloy carbides. It is well defined that in pearlite of alloyed steel the cementite can be replaced by other alloy carbides, such as $M_{23}C_6$ [25] or M_7C_3 [26]. The crystallography of the austenite–pearlite transformation in Fe–Cr–C alloys has been studied by Howell *et al.* [25]. In all cases the $M_{23}C_6$ carbide lamellae were related to the adjacent ferrite by the Kurdjumov–Sachs orientation relationship [27].

To the knowledge of the present authors, the crystallography of the pearlite with M_7C_3 carbide lamellae has not been studied in detail. Thus the present study was undertaken in order to reveal the habit plane and orientation relationship between pearlitic ferrite and M_7C_3 carbide in an Fe–8.2Cr–0.96C alloy.

2. EXPERIMENTAL PROCEDURE

2.1. Sample preparation

The chemical composition of the alloys used in the present investigation is shown in Table 1. Specimens of 20 mm in diameter and 10 mm long were austenitized at 1250°C for 15 min in a dynamic argon atmosphere. They were transformed isothermally in a lead bath covered with a layer of active charcoal to prevent decarburization at 725°C for 720 s, then quenched into iced brine. These heat treatments resulted in the lamellar pearlite containing M_7C_3 carbide lamellae with an average interlamellar spacing of about 0.1 μm.

The specimens for the microstructural investigations were sliced from the centre of each bulk specimen. Thin foils for TEM studies were prepared from 3 mm discs, ground to a thickness of about 0.05 mm and electropolished by a conventional twin-jet polishing method using electrolyte containing 10% perchloric acid, 20% glycerol and 70% ethanol. The foils were examined in a JEM-3010 transmission electron microscope operating at 300 kV.

2.2. Method for determining the habit plane

The accurate determination of the habit plane was fulfilled through large-angle tilting in the transmission electron microscope. This method is described in detail in Ref. [9]. Tilting toward a point where the boundary image is the sharpest results in the case when the electron beam is parallel to the habit plane. Once found the habit plane was further checked by tilting around an axis which was found to be normal to the habit plane. The zone axis is changed but the interface remains perpendicular to the tilting axis. Since there are many reflections on the line normal to the direction of a habit plane trace in the stereographic projection, one of them close to the reflecting zone can be accepted as a true habit plane normal. Thus such a procedure will exclude the erroneous interface normal.

Table 1. Chemical composition of the alloy (mass %)

C	Si	Mn	P	S	Cr	N	O	Al
0.96	0.02	0.001	0.001	0.001	8.24	0.0011	0.003	0.003

2.3. Structure of the M_7C_3 carbide

Selected area electron diffraction (SAED) patterns from the M_7C_3 carbide are generally complex because of the pseudo-hexagonal structure containing 56 iron atoms and 24 carbon atoms in a unit cell with lattice parameters $a = 1.3982$ nm and $c = 0.4506$ nm [28]. It has frequently been observed that the corresponding SAED patterns from the M_7C_3 carbide contain long streaks through the reciprocal lattice space perpendicular to $\{10\bar{1}0\}$ planes [29, 30]. These streaks result from a faulted structure with the fault vector being one half of the unit cell repeat distance [31]. The observed distribution of the diffuse intensity along the $\langle 11\bar{2}0\rangle$ directions in the Fe_7C_3 carbide has been attributed to a structure composed of ordered microdomains separated by non-periodic $\{11\bar{2}0\}$ defects [32]. In the present study, since the streaks were frequently observed along $\langle 11\bar{2}0\rangle$ and $\langle 1\bar{1}00\rangle$ directions, this phenomenon is thought to arise from the presence of defects in planes perpendicular to the basal plane. The structure of the M_7C_3 phase can also be interpreted as the orthorhombic crystal structure with $a = 0.4532$ nm, $b = 0.7015$ nm and $c = 1.2153$ nm as reported by Fruchart and Rouault [33] and was investigated in detail by Morniroli *et al.* [32].

3. EXPERIMENTAL RESULTS

A typical pearlite area with M_7C_3 carbide lamellae is shown in Fig. 1(a). The SAED pattern taken from the ferrite/carbide area [Fig. 1(c)] allows their crystallography to be determined. The stereographic analysis for this diffraction pattern is shown in Fig. 1(e). The incident beam direction is $[\bar{1}13]_b//[\bar{1}100]_{hex}$. (Hereafter, the subscripts b, f, hex and orth denote the b.c.c. structure of ferrite, the f.c.c. structure of austenite and the hexagonal or orthorhombic structure of the M_7C_3 phase, respectively.) Thus, the following orientation relationship between ferrite and M_7C_3 carbide was deduced:

$$[\bar{1}13]_b//[\bar{1}100]_{hex}$$

$$(25\bar{1})_b//(11\bar{2}0)_{hex}$$

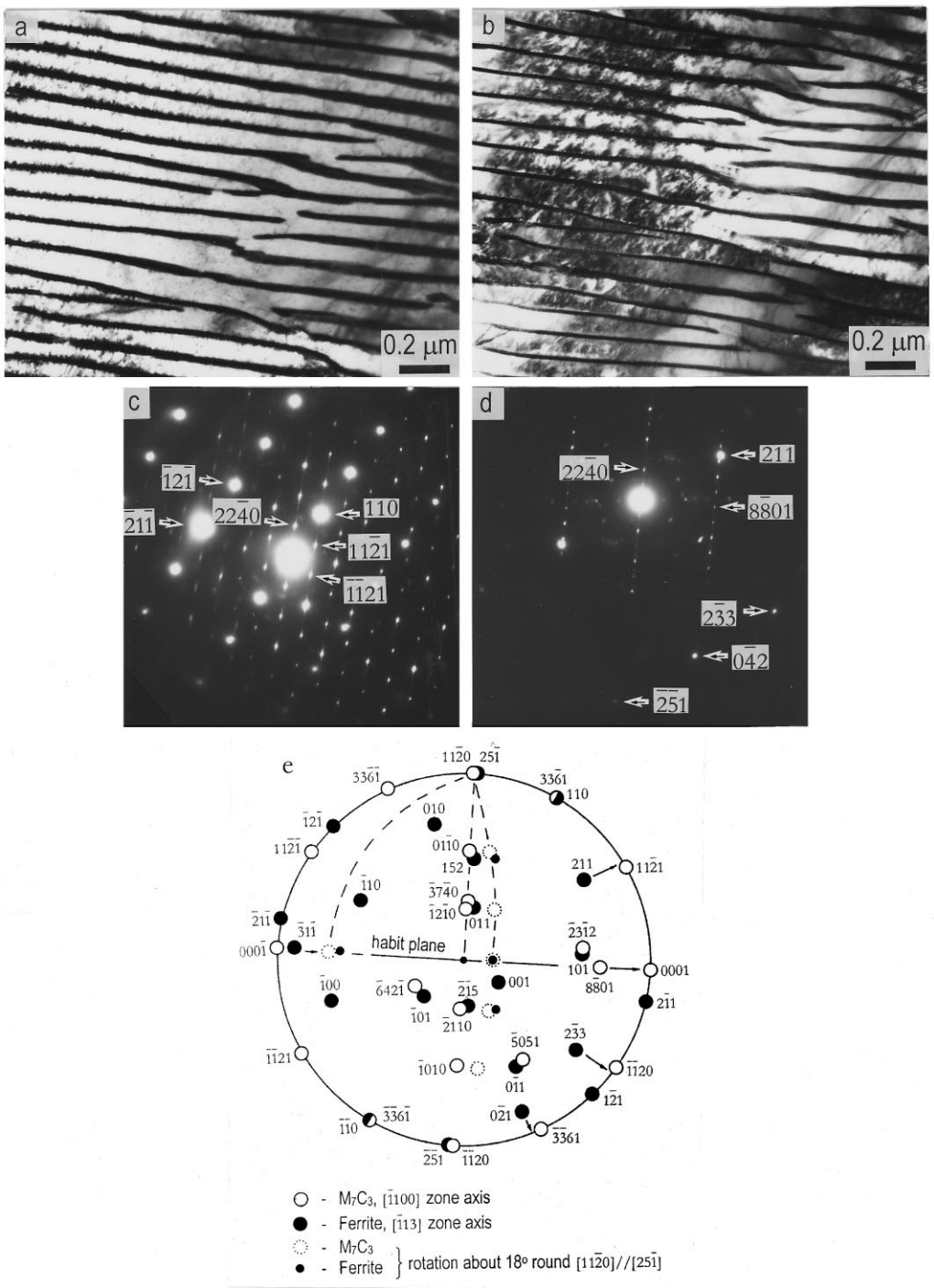

Fig. 1. TEM micrographs and corresponding SAED patterns from the same pearlite area tilted around $[25\bar{1}]_b//[11\bar{2}0]_{hex}$ at an angle of 17.9°: (a) and (c) $Z = [\bar{1}13]_b//[\bar{1}100]_{hex}$; (b) and (d) $Z = [\bar{3}24]_b$; (e) the $[\bar{1}13]_b//[\bar{1}100]_{hex}$ stereographic projection showing the habit plane and the OR-I between ferrite and M_7C_3 carbide.

$$(\bar{3}1\bar{1})_b \approx //(000\bar{1})_{hex}$$

The angle between $[25\bar{1}]_b$ and $[11\bar{2}0]_{hex}$ was determined to be about 1.5° whereas the $[\bar{3}1\bar{1}]_b$ is not strictly parallel to the $[000\bar{1}]_{hex}$. Thus the above expression for this orientation relationship is just an ideal approximation. This is termed the OR-I. The habit plane determined is the $(25\bar{1})_b//(11\bar{2}0)_{hex}$. However, with an orientation such as in Fig. 1(c), it is difficult to assert that the habit plane is not $(01\bar{1}0)_{hex}$ but $(11\bar{2}0)_{hex}$.

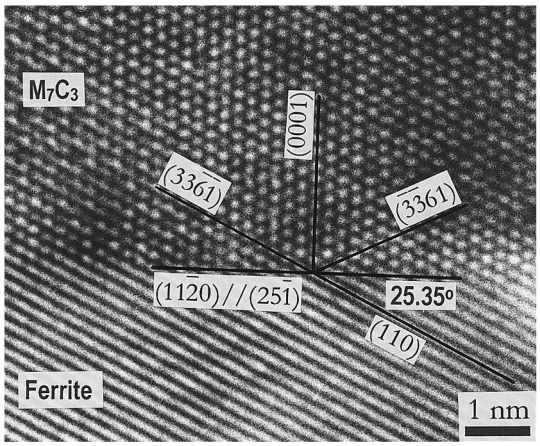

Fig. 2. HRTEM image of the edge of the M_7C_3 carbide lamella in the case of the OR-I. The incident beam direction is $[\bar{1}13]_b//[\bar{1}100]_{hex}$. The habit plane is $(25\bar{1})_b//(11\bar{2}0)_{hex}$.

Figures 1(b) and (d) are, respectively, a bright field image of pearlite and the corresponding SAED pattern taken after tilting around the axis $[25\bar{1}]_b//[11\bar{2}0]_{hex}$ on the angle of 17.9°. In this case the incident beam direction is $[\bar{3}24]_b$. The corresponding displacement of the ferrite and M_7C_3 carbide reflections is shown in the stereographic projection by arrows. From such an orientation it is rather easy to see that the habit plane is indeed the $(25\bar{1})_b//(11\bar{2}0)_{hex}$.

The HRTEM micrograph of Fig. 2 shows the atomic structure of the interphase boundary at the edge of the M_7C_3 carbide lamella. The corresponding SAED pattern is shown in Fig. 1(b). The incident beam is $[\bar{1}13]_b//[\bar{1}100]_{hex}$. In this figure, the ferrite/carbide interface is atomically flat. It can be seen that the M_7C_3 carbide habit plane is accurately parallel to the atomic habit plane $(25\bar{1})_b//(11\bar{2}0)_{hex}$. The $(110)_b$ ferrite close packed planes are parallel to the $(33\bar{6}\bar{1})_{hex}$ planes of the M_7C_3 phase and atomic planes are perfectly matched across this interface. Thus, this M_7C_3 carbide should maintain good coherency with respect to the matrix.

Figures 3(a) and (b) show the TEM micrographs of a pearlite area in different view directions. Their diffraction patterns and the summarized stereographic analysis are shown through Figs 3(c)–(e). The incident beam direction in Figs 3(a) and (c) is $[\bar{1}13]_b//[11\bar{2}0]_{hex}$ whereas Figs 3(b) and (d) were obtained through tilting around the axis $[\bar{2}\bar{5}1]_b//[1\bar{1}00]_{hex}$ through an angle of 25.5°. Such a tilting procedure once again allows the habit plane to be unambiguously recognized. The lamellar area in this case is parallel to the atomic habit plane $(\bar{2}\bar{5}1)_b//(1\bar{1}00)_{hex}$. The orientation relationship between ferrite and M_7C_3 carbide lamellae can be expressed as follows:

$$[\bar{1}13]_b//[11\bar{2}0]_{hex}$$

$$(\bar{2}\bar{5}1)_b//(1\bar{1}00)_{hex}$$

$$(\bar{3}1\bar{1})_b \approx //(0001)_{hex}$$

This is termed the OR-II. Similar to the OR-I, the angle between $[\bar{2}\bar{5}1]_b$ and $[1\bar{1}00]_{hex}$ was determined to be 1.5° but the $[\bar{3}1\bar{1}]_b$ is deviated from the $[0001]_{hex}$. These deviations were seen in all of the areas studied at different view directions although this orientation relationship itself obeys well. Note that the OR-II is identical to the orientation relation no. 2 for M_7C_3 carbide in ferrite after tempering of alloy steels reported by Dyson and Andrews [33].

Figure 4 is the HRTEM micrograph showing an edge-on view of the atomic structure of the broad face of the M_7C_3 carbide lamella. The incident beam direction is $[\bar{1}13]_b//[11\bar{2}0]_{hex}$. The corresponding SAED pattern is shown in Fig. 3(b). Note that in the ferrite area, only the $(110)_b$ lattice fringes can be seen. The angle between $(110)_b$ and $(25\bar{1})_b$ planes in ferrite is 25.35°, thus the $(25\bar{1})_b$ planes are almost parallel to the $(\bar{1}100)_{hex}$ planes. It can be seen that the $(110)_b$ planes are almost parallel to the $(5\bar{5}01)_{hex}$ and the atomic planes are perfectly matched across the interface suggesting good coherency, because extra half planes at the broad face of the M_7C_3 carbide lamella are not observed.

Figure 5 is a lattice image showing the $(101)_b$ planes of ferrite and $(1\bar{1}00)_{hex}$ planes of M_7C_3 carbide. This micrograph was taken at the diffraction conditions shown in Fig. 3(d). It can be seen that the ferrite habit plane deviates about 1.5° from the $(25\bar{1})_b//(1\bar{1}00)_{hex}$, which is the broad face on the habit plane. Figure 5 also shows that there are steps on both sides of the ferrite/carbide interface aligned in the growth direction of the carbide $[\bar{3}1\bar{1}]_b//[0001]_{hex}$. The step heights are one to three unit lattice heights of the M_7C_3 phase in the $[1\bar{1}00]_{hex}$ direction. These steps accommodate the divergence of the interface from the atomic habit plane, which is similar to that observed in the ferrite/cementite pearlite [2]. Note that the edge dislocation is visible within M_7C_3 carbide lamella. The core region of the extra half $(1\bar{1}00)_{hex}$ plane is shown in this figure by a circle.

Figure 6 is an HRTEM image showing a good atomic matching between the $(0\bar{1}1)_b$ close packed planes of ferrite and the $(4\bar{6}2\bar{1})_{hex}$ planes of the M_7C_3 carbide. The angle between them was determined to be about 2.5°.

Two sets of the bright field images and the corresponding SAED patterns in Fig. 7 show two different variants of the OR-II. In Figs 7(a) and (c) the incident beam is close to $[01\bar{1}]_b//[11\bar{2}1]_{hex}$. The stereographic projection in Fig. 7(e) shows that the OR-II is fulfilled within a few degrees as follows:

$$(\bar{5}\bar{1}\bar{2})_b//(1\bar{1}00)_{hex}$$

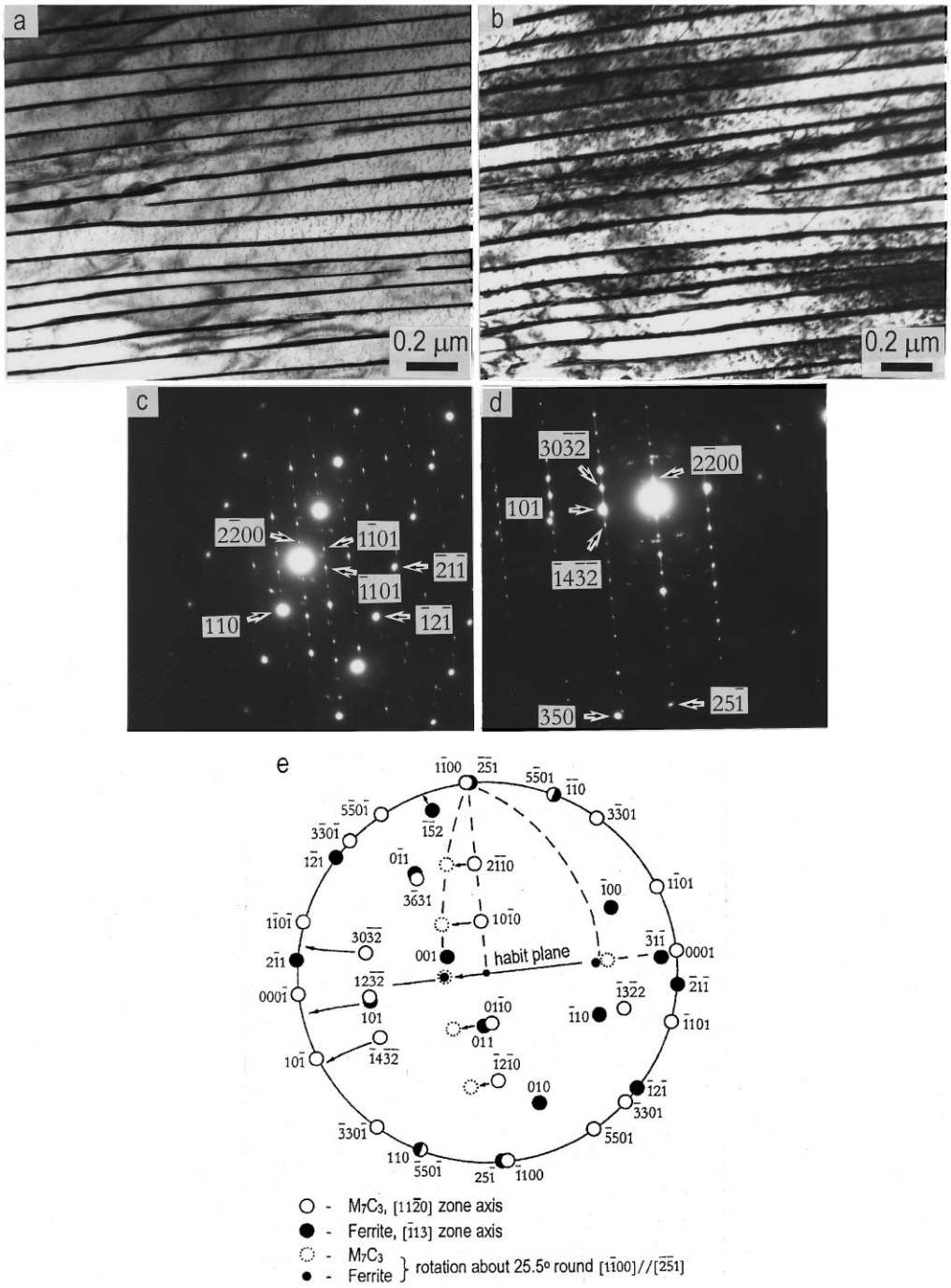

Fig. 3. TEM micrographs and corresponding SAED patterns from the same pearlite area tilted around $[\bar{2}\bar{5}1]_b//[1\bar{1}00]_{hex}$ at an angle of 25.5°: (a) and (c) $Z = [\bar{1}13]_b//[11\bar{2}0]_{hex}$; (b) and (d) $Z = [\bar{5}35]_b$; (e) the $[\bar{1}13]_b//[11\bar{2}0]_{hex}$ stereographic projection showing the habit plane and the OR-II between ferrite and M_7C_3 carbide.

$$(\bar{1}31)_b//(11\bar{2}0)_{hex}$$

$$(11\bar{3})_b \approx //(0001)_{hex}$$

The $[1,17,\overline{13}]_b$ zone axis shows even better correlation between ferrite and carbide reflections for the OR-II [as shown in Fig. 7(c) by arrows]. It can be easily seen that the habit plane of the carbide lamellae is $(\bar{5}\bar{1}\bar{2})_b//(1\bar{1}00)_{hex}$. Meanwhile, for the sake of clarity, the following discussion is more convenient to continue using the $[01\bar{1}]_b$ zone axis. Figures 7(b) and (d) are the bright field micrograph and the cor-

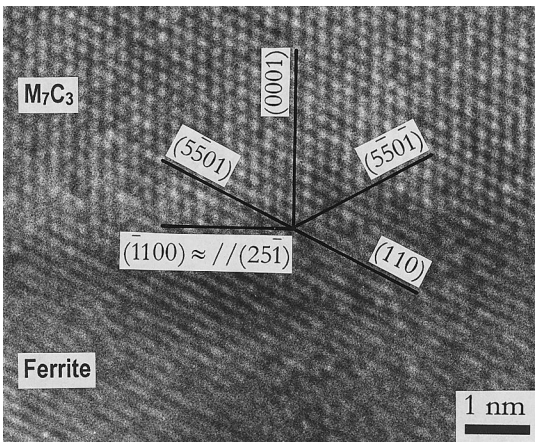

Fig. 4. HRTEM image of the edge of the M_7C_3 carbide lamella. The incident beam direction is $[\bar{1}13]_b//[11\bar{2}0]_b$. The habit plane is close to $(25\bar{1})_b//(\bar{1}100)_b$.

responding SAEDP taken from aother pearlite colony. The incident beam direction is again close to $[01\bar{1}]_b//[11\bar{2}1]_{hex}$. The habit plane can be safely recognized as $(152)_b//(\bar{1}100)_{hex}$. The orientation of the M_7C_3 carbide lamella is almost the same as in Fig. 7(c), but the ferrite is rotated about 45° around the $[01\bar{1}]_b$. The stereographic projection in Fig. 7(e) shows the other variant of the OR-II, namely

$$(5\bar{1}\bar{2})_b//(\bar{1}100)_{hex}$$

$$(131)_b//(11\bar{2}0)_{hex}$$

$$(\bar{1}1\bar{3})_b \approx //(0001)_{hex}$$

Figure 8 is just one more example of the OR-II:

$$(2\bar{1}\bar{5})_b//(\bar{1}100)_{hex} \text{ habit plane}$$

$$(311)_b//(\bar{1}\bar{1}20)_{hex}$$

$$(1\bar{3}1)_b \approx //(0001)_{hex}$$

Finally, it should be mentioned that the two orientation relationships reported above were observed in 15 different pearlite colonies. The OR-II was observed somewhat more often than OR-I and no other orientation relationships were observed.

4. DISCUSSION

4.1. Ferrite/carbide crystallography

In the present study, the crystallography and atomic structure of the interfaces in the ferrite/M_7C_3 pearlite was studied. The experimental observations described above can be summarized as follows.

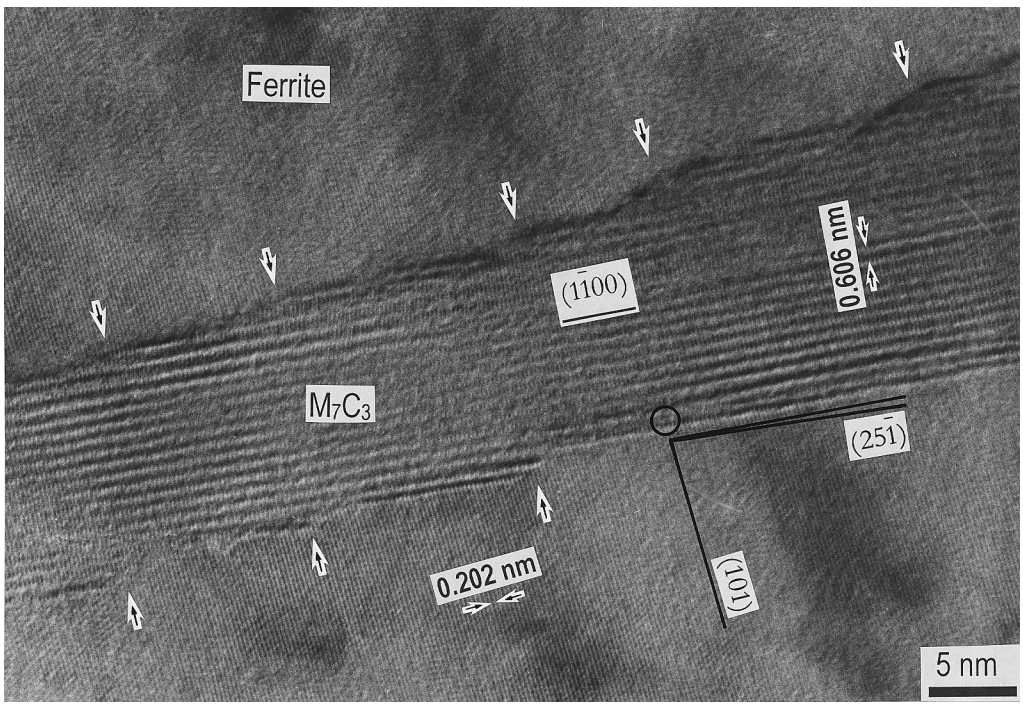

Fig. 5. TEM micrograph showing the $(101)_b$ ferrite and $(1\bar{1}00)_b$ M_7C_3 carbide lattice image. The incident beam direction is close to $[\bar{5}35]_b$. The habit plane deviates by 1.5° from the $(25\bar{1})_b//(1\bar{1}00)_b$. The growth steps are shown by arrows. The core region of the edge dislocation is shown by a circle.

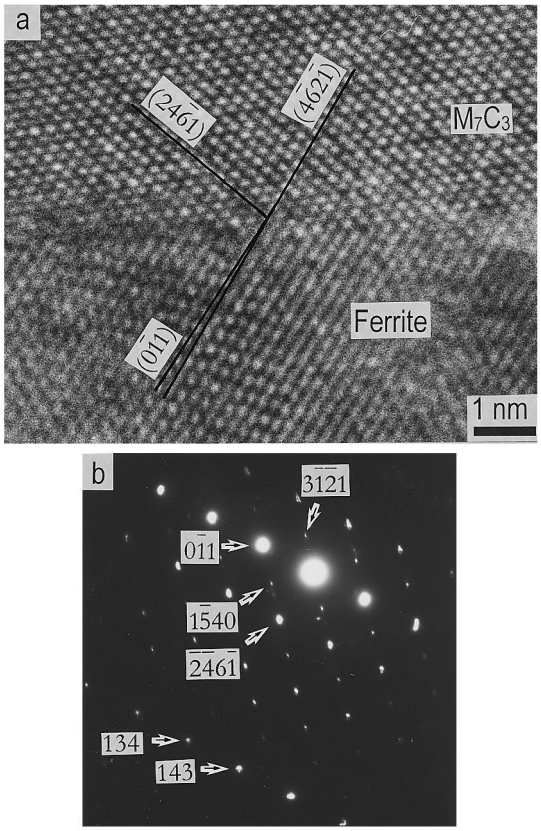

Fig. 6. (a) HRTEM image of the ferrite/carbide interface and (b) the corresponding SAED pattern. The incident beam direction is close to $[\bar{7}11]_b$.

1. The ferrite/M_7C_3 pearlite mainly grows along $[311]_b//[0001]_{hex}$.
2. Two specific orientation relationships were found to exist between the M_7C_3 carbide lamellae and the ferritic matrix.
3. Each of these orientation relationships has a unique habit plane:

OR-I:

$$(\bar{2}\bar{5}1)_b//(11\bar{2}0)_{hex} \text{ habit plane}$$

$$(\bar{1}13)_b//(\bar{1}100)_{hex}$$

$$(\bar{3}1\bar{1})_b \approx //(0001)_{hex}$$

OR-II:

$$(\bar{2}\bar{5}1)_b//(1\bar{1}00)_{hex} \text{ habit plane}$$

$$(\bar{1}13)_b//(11\bar{2}0)_{hex}$$

$$(\bar{3}1\bar{1})_b \approx //(0001)_{hex}$$

Since the angle between $(311)_b$ and $(521)_b$ is 7.75°, both orientation relationships are very close but the habit planes are quite different. Because of the hexagonal symmetry of the M_7C_3 phase, its three $\{10\bar{1}0\}_{hex}$ planes and three $\{2\bar{1}\bar{1}0\}_{hex}$ planes are equivalent. Thus the OR-I and OR-II can be obtained by a rotation of 30° about their common axis $[\bar{3}1\bar{1}]_b \approx //[0001]_{hex}$ to one another.

4. In the case of the OR-II, the habit plane was observed to deviate about 1.5° from the $(\bar{2}\bar{5}1)_b//(1\bar{1}00)_{hex}$.
5. The ferrite close packed planes were observed to be within a few degrees of the $(\bar{5}051)_{hex}$, $(33\bar{6}1)_{hex}$ or $(24\bar{6}1)_{hex}$ planes of the M_7C_3 carbide lamella. Across the interface, these planes are matched with perfect coherency, since the interface does not contain extra half planes.
6. The growth of the pearlite is accompanied by steps at the broad face of the M_7C_3 carbide lamella.

For further consideration of the orientation relationships between ferrite and M_7C_3 carbide, it is useful to express the structure of the M_7C_3 phase as orthorhombic. Using the convention $a = 0.4532$ nm, $b = 0.7015$ nm and $c = 1.2153$ nm reported by Fruchart and Rouault [34], the OR-I and OR-II can be expressed as follows:

OR-I:

$$(\bar{2}\bar{5}1)_b//(010)_{orth} \text{ habit plane}$$

$$(\bar{1}13)_b//(001)_{orth}$$

$$(\bar{3}1\bar{1})_b \approx //(100)_{orth}$$

OR-II

$$(\bar{2}\bar{5}1)_b//(001)_{orth} \text{ habit plane}$$

$$(\bar{1}13)_b//(010)_{orth}$$

$$(\bar{3}1\bar{1})_b \approx //(100)_{orth}$$

It is important to emphasize that the OR-II is similar to the Pitsch–Petch orientation relationship, which was often observed between ferrite and cementite in pearlite. For the sake of completeness,

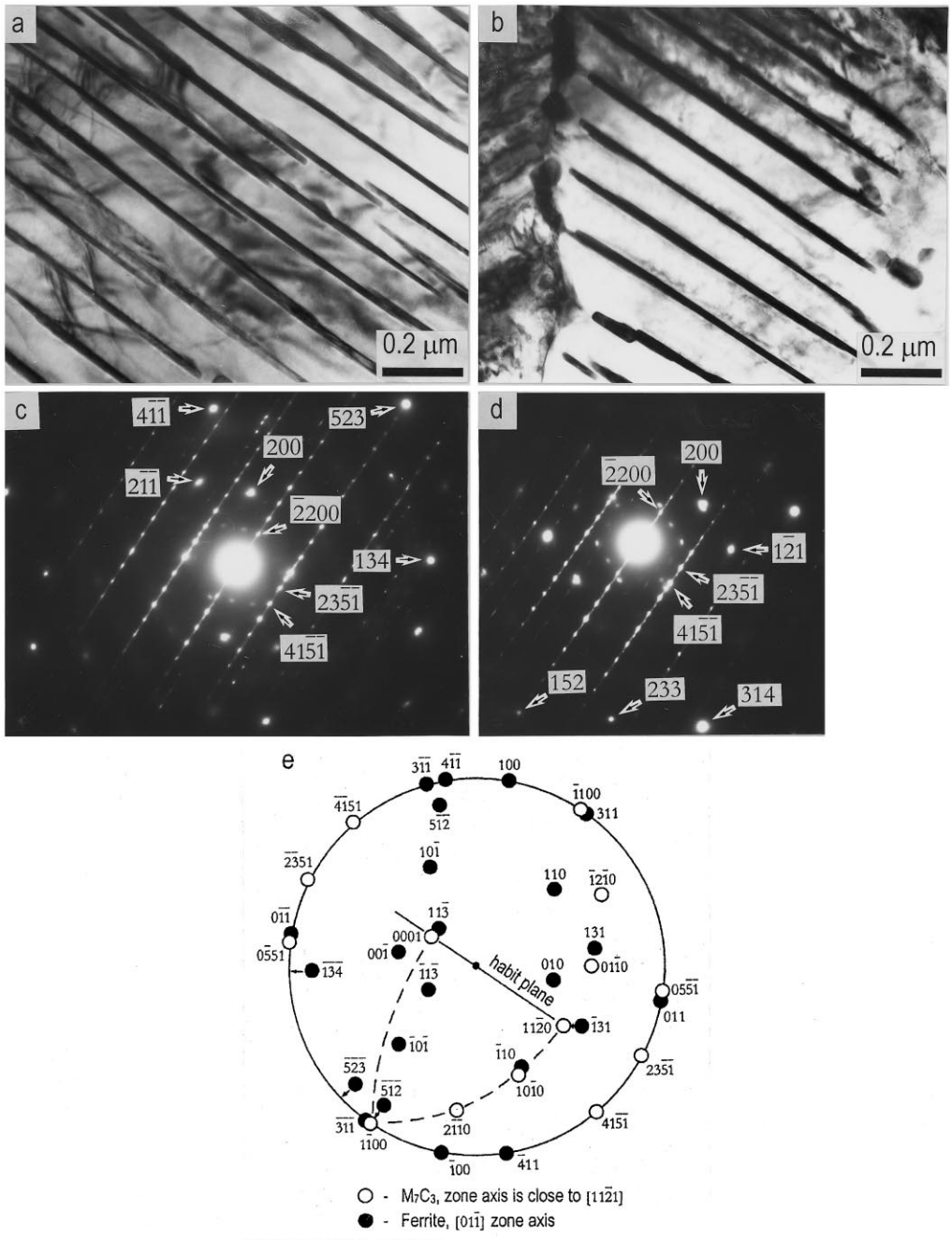

Fig. 7. TEM micrographs and corresponding SAED patterns from the different pearlite colonies showing the two variants of the OR-II. The incident beam direction is $[01\bar{1}]_b//[11\bar{2}1]_{hex}$. (e) The $[01\bar{1}]_b//[11\bar{2}1]_{hex}$ stereographic projection. Arrows show the displacements of the ferrite reflections by tilting from the $[01\bar{1}]_b$ to the $[1,17,\overline{13}]_{hex}$ zone axis.

it should be noted that the structure of cementite can also be described as hexagonal [35, 36].

It has been shown by Ohmori *et al.* [22] and confirmed by Zhou and Shiflet [9] that the Pitsch–Petch orientation relationship yields low interface energy. Minimization of interface energy is considered as one of the most important factors of the fixed orientation relationship and a one-to-one correspondence between the habit plane and orientation relationship. Minimization of strain energy at the interface requires good atomic matching. Zhang and Kelly [11, 37, 38] suggested that the orientation

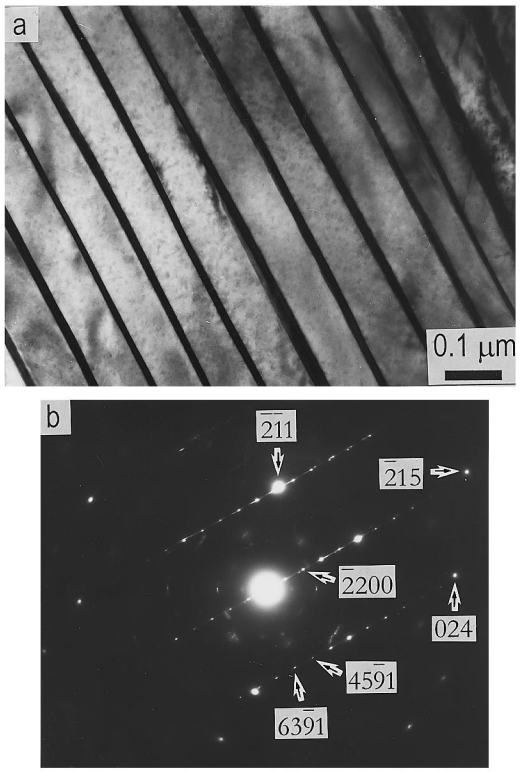

Fig. 8. (a) TEM micrograph and (b) the corresponding SAED pattern in the case of the OR-II. The incident beam direction is close to $[\bar{3}4\bar{2}]_b$. The habit plane is $(\bar{2}51)_b//(\bar{1}100)_{hex}$.

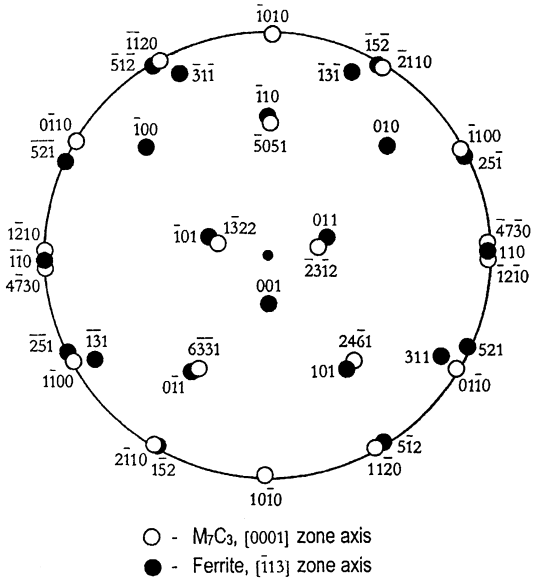

Fig. 9. The $[\bar{1}13]_b//[0001]_{hex}$ stereographic projection showing small misorientations between the $\{011\}_b$ ferrite planes and the coincident planes of the M_7C_3 phase in the case of the OR-I and OR-II. The d spacing of the matching planes are given in Table 2.

relationships should be expressed in terms of the close packed planes that show good atomic matching.

Figure 9 represents the stereographic projection on which the common axis for the OR-I and OR-II parallel to the growth direction of the pearlite lamellae is fixed. The OR-I or OR-II can simultaneously be expressed as follows:

OR-I:

$$(5\bar{1}2)_b//(11\bar{2}0)_{hex}$$

$$(\bar{1}\bar{3}1)_b//(1\bar{1}00)_{hex}$$

$$[\bar{1}13]_b \approx //[0001]_{hex}$$

OR-II

$$(25\bar{1})_b//(\bar{1}100)_{hex}$$

$$(\bar{3}1\bar{1})_b//(\bar{1}\bar{1}20)_{hex}$$

$$[\bar{1}13]_b \approx //[0001]_{hex}$$

The stereographic projection also shows that each of the $\{110\}_b$ close packed planes of ferrite is within a few degrees of one of the following planes in the M_7C_3 phase: $\{1\bar{3}22\}_{hex}$, $\{\bar{5}051\}_{hex}$, $\{33\bar{6}1\}_{hex}$, $\{6\bar{2}\bar{4}1\}_{hex}$, $\{7\bar{3}\bar{4}0\}_{hex}$ or $\{10\bar{1}0\}_{hex}$. Each of these planes has the d spacing close to that of the $(110)_b$ ferrite. The lattice misfits between these planes of the M_7C_3 phase and the $(110)_b$ planes of ferrite are summarized in Table 2. It can be seen that even the largest misfit does not exceed 5% whereas it is less than 2% in most cases.

Table 2. Lattice misfit between ferrite and M_7C_3 carbide planes

$(hkl)_h$	Lattice spacing, d_1 (nm)	$(hlk)_b$	Lattice spacing, d_2 (nm)	$(d_1-d_2)/d_1$
$\{50\bar{5}1\}$	0.213			0.047
$\{6\bar{3}\bar{3}1\}$	0.207			0.019
$\{6\bar{2}\bar{4}1\}$	0.204	{011}	0.203	0.005
$\{3\bar{1}\bar{2}2\}$	0.202			−0.005
$\{7\bar{3}40\}$	0.199			−0.020
$\{10\bar{1}0\}$	1.211/6 = 0.202			−0.0005

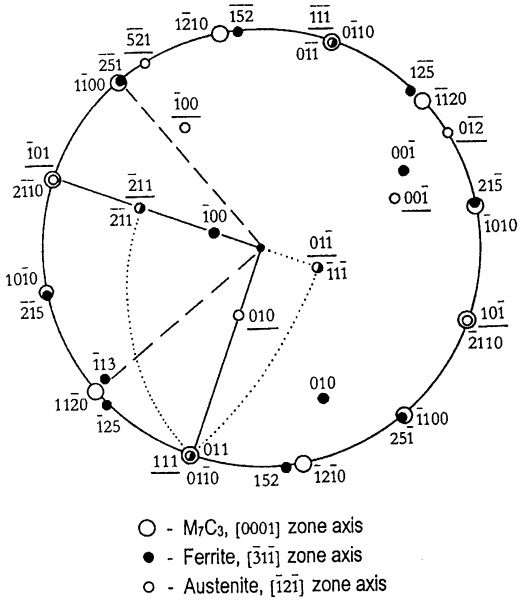

Fig. 10. The $[\bar{3}1\bar{1}]_b//[\bar{1}2\bar{1}]_f//[0001]_{hex}$ stereographic projection showing the orientation relationship between the austenite and M_7C_3 carbide in the case of the OR-I and OR-II if the Kurdjumov–Sachs orientation relationship between the ferrite and austenite is assumed.

The 30° rotation around the common axis $[\bar{1}13]_b \approx //[0001]_{hex}$ yields 12 variants of either orientation relationship. Note that only in half of them is the $\{2\bar{1}10\}_{hex}$ close packed plane of the hexagonal M_7C_3 phase less than 2.5° to the close packed plane $(110)_b$ of ferrite as shown in Fig. 9. It is obvious from the experimental observations [compare Fig. 1(e) with Fig. 3(e) and Fig. 7(e)] that the last condition is not strictly fulfilled.

4.2. Austenite/pearlite crystallography

The orientation relationships between the austenite and the two constituents of pearlite are also very important to observe the crystallography of the pearlite reaction as a whole. In the classical theory of pearlite growth developed by Smith [39] and Hillert [16], it is implicitly assumed that either of the pearlite constituents has no reproducible orientation relationship with the austenite grain it was growing into and the austenite/pearlite interface is disordered. This conclusion was supported by a number of other studies [40, 41]. Meanwhile, it has been shown by Shackleton and Kelly [42] that if the Pitsch austenite–cementite relationship and the Kurdjumov–Sachs austenite–ferrite relationship are assumed then the ferrite and cementite can be related by the Bagaryatskii orientation relationship within a few degrees.

Figure 10 represents the stereographic projection when the zone axis is $[\bar{3}1\bar{1}]_b//[\bar{1}2\bar{1}]_f//[0001]_{hex}$. The OR-II found in the present study is shown by dashed lines. If we assume that the ferritic pearlite and austenite are related by the Kurdjumov–Sachs relationship (as shown by dotted lines), the following orientation relationship between the austenite and M_7C_3 carbide can be deduced (shown by solid lines):

$$(111)_f//(01\bar{1}0)_{hex}$$

$$(\bar{1}01)_f//(2\bar{1}\bar{1}0)_{hex}$$

$$(\bar{1}2\bar{1})_f//(0001)_{hex}$$

If the orthorhombic symmetry of the M_7C_3 phase is adopted this orientation relationship can be rewritten as follows:

$$(111)_f//(001)_{orth}$$

$$(\bar{1}01)_f//(010)_{orth}$$

$$(\bar{1}2\bar{1})_f//(100)_{orth}$$

This orientation relationship is quite similar to the Pitsch orientation relationship in the case of cementite precipitation in austenite. Although this orientation relationship should experimentally be confirmed, it should be noted that, if this is true, the austenite/pearlite interface becomes coherent. The recent results by Hackney and Shiflet [10] also indicated the partial coherency at the austenite/ferrite/cementite interfaces despite the fact that rational orientation relationships are seldom confirmed.

5. SUMMARY

The crystallography and ferrite/carbide interface structure of pearlite with M_7C_3 carbide lamellae have been investigated by means of TEM using an SAED pattern technique. The following results were obtained.

1. In pearlite, two orientation relationships between ferrite and the M_7C_3 phase have been determined. Each of them has a unique atomic habit plane:

OR-I:

$$(\bar{2}\bar{5}1)_b//(11\bar{2}0)_{hex} \text{ habit plane}$$

$$(\bar{1}13)_b//(\bar{1}100)_{hex}$$

$$(\bar{3}1\bar{1})_b \approx //(0001)_{hex}$$

OR-II:

$$(\bar{2}\bar{5}1)_b//(1\bar{1}00)_{hex} \text{ habit plane}$$

$$(\bar{1}13)_b//(11\bar{2}0)_{hex}$$

$$(\bar{3}1\bar{1})_b \approx //(0001)_{hex}$$

2. In the case of the OR-II, the habit plane of an M_7C_3 carbide lamella deviates by 1.5° from the $(\bar{2}\bar{5}1)_b//(1\bar{1}00)_{hex}$.
3. The misorientation between the close packed planes of ferrite and the coincident planes of M_7C_3 carbide is always within a few degrees and atomic planes are perfectly matched through the interface. This implies that both pearlite constituents form coherently to one another.

Acknowledgements—D. Shtansky acknowledges the support of the Japan Society for the Promotion of Science during this work. This research was supported by the Grant-in-Aid of The Ministry of Education, Science, Culture and Sports. Thanks are also due to Sumitomo Metal Industries for supplying the materials used in the present study.

REFERENCES

1. Hackney, S.A. and Shiflet, G.J., *Acta metall.*, 1987, **35**, 1019.
2. Zhou, D.S. and Shiflet, G.J., *Metall. Trans.*, 1991, **22A**, 1349.
3. Whiting, M.J. and Tsakiropoulos, P., *Scripta metall.*, 1993, **29**, 401.
4. Whiting, M.J. and Tsakiropoulos, P., *Scripta metall.*, 1994, **30**, 1031.
5. Sharma, R.C., Purdy, G.R. and Kirkaldy, J.S., *Metall. Trans.*, 1979, **10A**, 1129.
6. Kennon, N.F., *Metall. Trans.*, 1978, **9A**, 57.
7. Razik, N.A., Lorimer, G.W. and Ridley, N., *Metall. Trans.*, 1976, **7A**, 209.
8. Tewari, S.K. and Sharma, R.C., *Metall. Trans.*, 1985, **16A**, 597.
9. Zhou, D.S. and Shiflet, G.J., *Metall. Trans.*, 1992, **23A**, 1259.
10. Hackney, S.A. and Shiflet, G.J., *Acta metall.*, 1987, **35**, 1007.
11. Zhang, M.-X. and Kelly, P.M., *Scripta mater.*, 1997, **37**, 2009.
12. Ridley, N., *Metall. Trans.*, 1984, **15A**, 1019.
13. Hull, F.C. and Mehl, R.F., *Trans. Am. Soc. Metals*, 1942, **30**, 381.
14. Zener, C., *Trans. Am. Inst. Min. Engrs*, 1946, **167**, 550.
15. Mehl, R.F. and Hagel, W.C., *Prog. Metal Phys.*, 1956, **6**, 74.
16. Hillert, M., *Decomposition of Austenite by Diffusional Processes*. Interscience, New York, 1962, p. 197.
17. Whiting, M.J. and Tsakiropoulos, P., *Scripta metall.*, 1995, **32**, 1965.
18. Hillert, M., *Scripta metall.*, 1994, **31**, 1173.
19. Khalid, F.A. and Edmonds, D.V., *Acta mater.*, 1993, **41**, 3421.
20. Bagaryatskii, Y.A., *Dokl. Akad. Nauk SSSR*, 1950, **73**, 1161.
21. Isaichev, I.V., *Zh. Tekh. Fiz.*, 1947, **17**, 835.
22. Ohmori, Y., Davenport, A.T. and Honeycombe, R.W.K., *Trans. Iron Steel Inst. Japan*, 1972, **12**, 128.
23. Petch, N.J., *Acta crystallogr.*, 1953, **6**, 96.
24. Pitsch, W., *Acta metall.*, 1962, **10**, 79.
25. Howell, P.R., Bee, J.V. and Honeycombe, R.W.K., *Metall. Trans.*, 1979, **10A**, 1213.
26. Shtansky, D.V., Nakai, K. and Ohmori, Y., *Z. Metallk.*, 1999, **1**, 25.
27. Kurdjumov, G.V. and Sachs, G., *Z. Phys.*, 1930, **64**, 325.
28. Andrews, K.W., Dyson, D.J. and Koewn, S.R., *Interpretation of Electron Diffraction Patterns*. Adam Hilger, London, 1967, p. 188.
29. Beech, J. and Warrington, D.H., *J. Iron Steel Inst.*, 1966, **204**, 460.
30. Inoue, A. and Masumoto, T., *Matall. Trans.*, 1980, **11A**, 739.
31. Honeycombe, R.W.K., in *Metallography*, ISI Special Report, Vol. 80, 1963, p. 245.
32. Morniroli, J.P., Bauer-Grosse, E. and Gantois, M., *Phil. Mag. A*, 1983, **48**, 311.
33. Dyson, D.J. and Andrews, K.W., *J. Iron Steel Inst.*, 1969, **207**, 208.
34. Fruchart, M.R. and Rouault, M.A., *Ann. Chim.*, 1969, **4**, 143.
35. Lipson, H. and Petch, N.J., *J. Iron Steel Inst.*, 1940, **142**, 95.
36. Fasiska, E.J. and Jeffrey, G.A., *Acta crystallogr.*, 1965, **19**, 463.
37. Zhang, M.-X. and Kelly, P.M., *Scripta metall.*, 1997, **37**, 2017.
38. Zhang, M.-X. and Kelly, P.M., *Acta mater.*, 1998, **46**, 4617.
39. Smith, C.S., *Trans. Am. Soc. Metals*, 1953, **45**, 533.
40. Smith, C.S. and Mehl, R.F., *Trans. Aam. Inst. Min. Engrs*, 1942, **150**, 211.
41. Dippenaar, R.J. and Honeycombe, R.W.K., *Proc. R. Soc. A*, 1973, **333**, 455.
42. Shackleton, D.N. and Kelly, P.M., *Acta metall.*, 1967, **15**, 979.